Applied Catalysis B: Environmental 181 (2016) 495–503

Contents lists available at ScienceDirect

Applied Catalysis B: Environmental

journal homepage: www.elsevier.com/locate/apcatb

Engineering the Cu_2O–reduced graphene oxide interface to enhance photocatalytic degradation of organic pollutants under visible light

Weixin Zou[a,b], Lei Zhang[a,b], Lichen Liu[a,b], Xiaobo Wang[a,b], Jingfang Sun[b], Shiguo Wu[a,b], Yu Deng[b], Changjin Tang[a,b], Fei Gao[a,b,*], Lin Dong[a,b,*]

[a] Key Laboratory of Mesoscopic Chemistry of MOE, School of Chemistry and Chemical Engineering, Nanjing University, Nanjing 210093, PR China
[b] Jiangsu Key Laboratory of Vehicle Emissions Control, Center of Modern Analysis, Nanjing University, Nanjing 210093, PR China

ARTICLE INFO

Article history:
Received 23 May 2015
Received in revised form 3 August 2015
Accepted 9 August 2015
Available online 12 August 2015

Keywords:
Crystal-plane effect
Cu_2O–rGO
Visible-light degradation
Superoxide radical
Interfacial interaction

ABSTRACT

In this work, Cu_2O–reduced graphene oxide (rGO) composites were synthesized with tunable Cu_2O crystal facets ({1 1 1}, {1 1 0} and {1 0 0} facets). The degradation performance of methylene blue under visible light was ranked: o-Cu_2O{1 1 1}–rGO > d-Cu_2O{1 1 0}–rGO > c-Cu_2O{1 0 0}–rGO. UV–vis diffuse reflectance and photoluminescence spectra showed that o-Cu_2O–rGO exhibited the enhanced visible-light absorption and the faster charge-transfer rate. Furthermore, X-ray photoelectron spectroscopy and Raman characterizations showed that o-Cu_2O–rGO was beneficial for the stabilization of Cu^+ species and the formation of oxygen defects. With the help of *in-situ* electron spin resonance (ESR), more superoxide radicals were detected over o-Cu_2O–rGO, which promoted organic pollutants degradation. The above results confirmed that the catalytic behaviors of three Cu_2O–rGO composites were related to the electronic structures and interfacial connections. The o-Cu_2O{1 1 1}–rGO displayed the superior performance, for the highly-active coordinated unsaturated Cu and the intensive interfacial connection, which was beneficial for the rapid the photo-generated electron transfer and the formed active superoxide species. This study showed that engineering the interfacial structures could provide a scientific basis for the design of efficient photo-catalysts.

1. Introduction

With the rapid development of modern industry, the environmental pollution (especially organic dye pollutants) threatens human health, and thus, the pollutant elimination has become one of the most important research fields [1–3]. Photo-catalytic degradation under solar light is believed as one of the most promising strategies, based on the global energy crisis and the sustainability and renewability of solar light. In recent years, cuprous oxide (Cu_2O) nanocrystals with different exposed crystal facets (cube with {1 0 0} facet, octahedron with {1 1 1} facet, rhombic dodecahedron with {1 1 0} facet) for photo-catalytic reactions have been extensively studied [4,5]. However, the wide application of traditional Cu_2O nanocrystals is limited by many factors, including the poor stability in oxidizing environments, rapid recombination of photo-generated electrons and holes, and transformation of crystal planes under reaction process [6–8]. Therefore, various materials (n-type semiconductors [9], noble metals [10,11], and carbon materials [12,13]) are employed to modify the traditional Cu_2O crystals, for the purpose of photo-catalytic performance enhancement. Graphene or reduced graphene oxide (rGO), a promising material with a range of unique properties (superior mobility of charge carriers, extremely high specific surface area and excellent conductivity) [14–16], has recently acted as a flexible conducting support to encapsulate Cu_2O nanocrystals in many fields [17–19]. Tran et al. prepared Cu_2O–reduced graphene oxide (Cu_2O–rGO) nanocomposite, and discovered that due to the formation of *p–n* Cu_2O–rGO junction, the prepared Cu_2O–rGO nanocomposite had the superior photo-catalytic activity for hydrogen production under visible light [20].

Although studies on the photo-catalytic performance of Cu_2O–rGO have been reported, there are still some unanswered fundamental questions. Generally, different crystal facets with different atomic structures had significant influence on the electronic properties of semiconductor nanocrystals [9,21]. Zhang et al. reported that Cu_2O with more high-index facets exhibited better performance in photo-catalytic H_2 production, for the reason that photo-generated electrons preferred on high index planes, while

* Corresponding authors at: Key Laboratory of Mesoscopic Chemistry of MOE, School of Chemistry and Chemical Engineering, Nanjing University, Nanjing 210093, PR China. Fax: +86 25 83317761.
E-mail addresses: gaofei@nju.edu.cn (F. Gao), donglin@nju.edu.cn (L. Dong).

http://dx.doi.org/10.1016/j.apcatb.2015.08.017
0926-3373/

holes tended to migrate to low index planes [22]. Furthermore, our previous study discovered that TiO_2{1 0 0}-graphene showed the best activity in photo-catalytic H_2 production, because of the Ti—C bonds between {1 0 0} facet and graphene, which suggested that the interfacial structures of composites played a key role in the photo-catalysis [21]. Therefore, it is essential to investigate the interfacial charge–transfer interactions between reduced graphene oxide and Cu_2O with different crystal facets, which can provide a scientific basis for the design of efficient photo-catalysts.

In this work, a facile method was developed to synthesize Cu_2O–reduced graphene oxide (rGO) composites with different crystal facets. Cu_2O nanocrystals ({1 1 1}, {1 1 0}, {1 0 0} facets) were *in-situ* anchored on rGO sheets. The photo-degradation of methylene blue (MB) under visible light over Cu_2O–rGO composites were carried on, o-Cu_2O{1 1 1}–rGO had better performance than the two other composites. Photoluminescence (PL) and Fourier transform infrared (FT-IR) results demonstrated the stronger charge–transfer interactions on the interface of o-Cu_2O{1 1 1}–rGO composite. Furthermore, X-ray photoelectron spectroscopy (XPS), Raman and *in-situ* electron spin resonance (ESR) characterizations indicated that the electronic structures and interfacial connections between o-Cu_2O {1 1 1} and rGO sheet were advantageous, which was beneficial for the generated active superoxide radicals $O_2^{\bullet-}$ and the MB degradation. The schematic illustration of possible interfaces between Cu_2O crystals and rGO sheet was proposed, as well as the process of photo-degradation.

2. Experimental

2.1. Catalyst preparation

The o-Cu_2O{1 1 1}–rGO and c-Cu_2O{1 0 0}–rGO composites were prepared with $CuCl_2$ precursor. Graphene oxide (50 mg, Nanjing JicangNano Co., Ltd.) was ultrasonically dispersed in 50 mL $CuCl_2$ aqueous solution (0.01 mol/L). Polyvinylpyrrolidone (PVP, MW = 30,000) (octahedrons: 4.44 g; cubes: 0 g) were dissolved in the mixture under vigorous stirring for 1 h. NaOH aqueous solution (2.0 mol/L, 5.0 mL) was added dropwise at different temperatures (octahedrons: 55 °C; cubes: 60 °C). After 0.5 h, 5.0 mL ascorbic acid (Vc) aqueous solution (octahedrons: 0.6 g; cubes: 0.7 g) was dripped and the solution was stirring continuously (octahedrons: 3 h; cubes: 5 h) at the mentioned reaction temperatures. Finally, the obtained precipitate was collected by centrifugation, washed by excessive distilled water, absolute ethanol in ultrasound for several times to remove the ions and surfactant, and then dried in vacuum at 50 °C for 12 h.

The d-Cu_2O{1 1 0}–rGO composite were prepared with $CuSO_4$ precursor. Firstly, 0.5 mmol $CuSO_4$ was dissolved well in 18 mL distilled water at the room temperature, and 50 mg graphene oxide was ultrasonically dispersed in the $CuSO_4$ solution. Secondly, 2 mL oleic acid and 12 mL absolute ethanol were added successively into the mixture with vigorous stirring. Thirdly, when the temperature reached 100 °C, 5 mL NaOH solution (0.8 mol/L) was added dropwise, and 15 mL D-(+)-glucose aqueous solution (1.71 g) was dropped after 5 min. The mixture above reacted for another 60 min. Finally, the obtained precipitate was collected by centrifugation, washed by excessive cyclohexane and absolute ethanol in ultrasound for several times to remove oleic acid, and dried in vacuum at 50 °C for 12 h.

2.2. Catalyst characterization

Scanning electron microscopy (SEM) experiments were performed on Philips XL30 electron microscope operated at beam energy of 10.0 kV. Transmission electron microscopy (TEM) images were taken on a JEM-2100 instrument at an acceleration voltage of 200 kV. The samples were crushed and dispersed in A.R. grade ethanol and the resulting suspensions were allowed to dry on carbon film supported on copper grids. Powder X-ray diffraction (XRD) patterns were recorded on a Philips X'pert Pro diffraction using Ni-filtered Cu Kα radiation (λ = 0.15418 nm). The X-ray tube was operated at 40 kV and 40 mA and the intensity data were collected over a 2θ range of 5–90°. The scan speed was set at 6° min^{-1} with a step size of 0.02°. Brunauer–Emmet–Teller (BET) surface areas were measured by nitrogen adsorption at 77 K on a Micrometrics ASAP-2020 adsorption apparatus. Before each adsorption measurement, approximate 0.1 g sample was degassed in a N_2/He mixture at 200 °C for 3 h. UV–vis diffuse reflectance spectroscopy (UV–vis DRS) were recorded in the range of 200–800 nm by a Shimadzu UV–2401 spectrophotometer with $BaSO_4$ as reference. Photoluminescence (PL) spectra were measured at room temperature on an F-7000 fluorescence spectrophotometer (Hitachi, Japan). The wavelength of the excitation light was 360 nm. Fourier transform infrared (FT-IR) spectra were collected from 400 to 4000 cm^{-1} at a spectral resolution of 4 cm^{-1} (number of scans, 32) on a Nicolet 5700 FT-IR spectrometer equipped with a high-sensitive MCT detector cooled by liquid N_2. X-ray photoelectron spectroscopy (XPS) analysis was performed on a PHI 5000 Versa Probe system, using monochromatic Al Kα radiation (1486.6 eV) operating at an accelerating power of 15 kW. Before the measurement, the sample was outgassed at room temperature in a UHV chamber ($<5 \times 10^{-7}$ Pa). The sample charging effects were compensated by calibrating all binding energies (BE) with the adventitious C 1 s peak at 284.6 eV. This reference gave BE values with accuracy at ±0.1 eV. Raman spectra were recorded by using a Renishaw *in via* spectrometer. Raman excitation at 514.5 nm was provided by Ar^+ laser. A laser power of 20 mW at the sample was applied. The electron spin resonance (ESR) signals of radicals spin-trapped by spin-trap reagent 5,5′-dimethyl-1-pirroline-*N*-oxide (DMPO) (purchased from Sigma Chemical Co.) were examined on a Bruker model ESR JES FA200 (JEOL) spectrometer. The superoxide radicals were obtained from direct measurements of magnetic field and microwave frequency at 77 K under visible light.

2.3. Photocatalytic performances test

The photocatalytic performances of the Cu_2O–rGO and Cu_2O catalysts for the methylene blue (MB) degradation were measured under the visible light. The visible light ($\lambda \geq 420$ nm) was provided by the 400 W metal halide lamp equipped with an ultraviolet cut-off filter. The sample (15 mg) was added to 45 mL MB (10 mg L^{-1}) solution. Before the photocatalytic performances test, the mixture was stirred for 2 h in dark at room temperature until the adsorption–desorption equilibrium between MB and the catalysts was achieved. The heat effect in the illumination was minimized by condensed water. During the illumination, approximately 2 mL suspension was withdrawn at fixed intervals (20 min), and then analyzed by an UV–vis spectrophotometer (UV–3600 spectrometer). The photocatalytic activity of MB was calculated by the concentration (C/C_0) according to the absorbance (A/A_0) at 660 nm, where C_0 and A_0 were the concentration and adsorption of MB after the adsorption–desorption equilibrium.

3. Results and discussion

The phase structures of as-prepared Cu_2O–rGO composites and graphene oxide (GO) were characterized by XRD. From the XRD patterns of Cu_2O–rGO composites (Fig. 1), it was clearly seen that no other copper species (Cu or CuO) were detected, except the typical diffraction patterns of Cu_2O crystals, which were ascribed perfectly

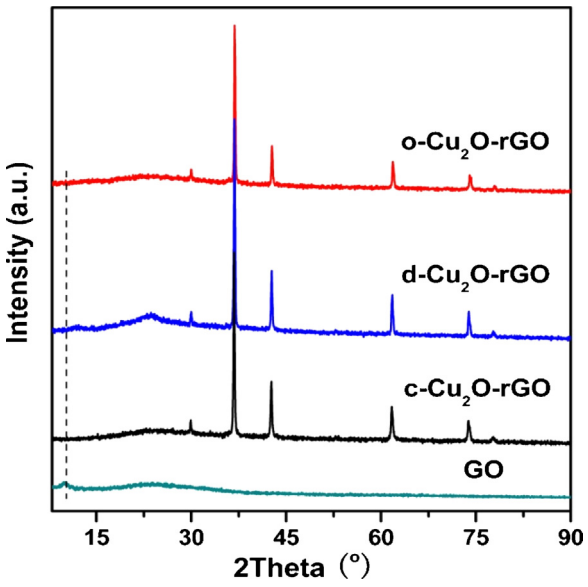

Fig. 1. XRD patterns of as-prepared Cu_2O–rGO composites and graphene oxide.

to the pure cubic-phase Cu_2O (JCPDS No. 65-3288, space group Pn3m, lattice constant $a = 0.4260$ nm) [23]. For graphene oxide, there was a peak at $2\theta = 10.3^\circ$ corresponding to the large interlayer distance, which suggested the present of epoxy, hydroxyl and carboxyl groups [24]. While, for Cu_2O–rGO composites, no diffraction peak belonging to graphene oxide could be observed, due to the reduction of graphene oxide in the synthesis, oxygen-containing functional groups were removed and the interlayer distance was decreased [12,25].

The morphologies of as-synthesized Cu_2O–rGO composites were investigated by SEM. As shown in Fig. 2, octahedral, dodecahedral and cubic Cu_2O nanocrystals were *in-situ* anchored on rGO sheets. On the basis of the size distribution results, the particle sizes of o-, d-, c-Cu_2O crystals on rGO sheet were mainly in range of 300–400, 200–400, 200–400 nm, respectively. The well dispersion of Cu_2O nanocrystals on rGO sheets suggested that strong binding interactions might present between Cu_2O nanocrystals and rGO sheets. TEM images in Fig. S1a, c, e (in Supplementary material) further showed that well-defined Cu_2O nanocrystals were effectively dispersed on rGO sheets. High resolution TEM (HRTEM) were used to study the corresponding exposed crystal planes. In Fig. S1b, the lattice spacing was 0.243 nm corresponding to {1 1 1} facets, which showed that Cu_2O octahedrons with {1 1 1} facets were formed. According to Fig. S1d, the dominant crystal facets of dodecahedral Cu_2O were {1 1 0} facets. In another Cu_2O–rGO composite, Cu_2O cubes could be observed on rGO sheets, as well as the lattice spacing of 0.212 nm for {2 0 0} facets (Fig. S1f). Based on the SEM and TEM results, it was demonstrated that Cu_2O–rGO composites with well-defined Cu_2O crystal facets had been successfully synthesized, and these composites were the ideal model photo-catalysts to study the crystal-plane effects on interfacial interactions.

The photo-catalytic activities of the as-prepared Cu_2O–rGO composites, using photo-degradation of methylene blue (MB) as the model reaction under visible-light irradiation, were displayed. The MB had been adsorbed by *ca.* 0.50, 0.35, 0.29 for o-Cu_2O–rGO, d-Cu_2O–rGO and c-Cu_2O–rGO after stirring 2 h in dark, respectively (Fig. S2a), and adsorption curves suggested that the adsorption–desorption equilibrium between MB and the catalysts was achieved. Afterward, the degree of degradation (C_t/C_0) as a function of irradiation time (C_0 was the concentration of MB after the adsorption–desorption equilibrium) was showed in Fig. 3a. It was found that in comparison with bare Cu_2O catalysts (Fig. S2b), the photo-degradation of MB was dramatically improved, indicating that the introduction of reduced graphene oxide promoted the photo-degradation process. Moreover, the degradation performances of three catalysts were different. The photo-degradation over o-Cu_2O–rGO, d-Cu_2O–rGO and c-Cu_2O–rGO catalysts were *ca.* 72%, 60% and 28% within 2 h, respectively. The photo-catalytic activity trend followed the order: o-Cu_2O–rGO > d-Cu_2O–rGO > c-Cu_2O–rGO. Clearly, o-Cu_2O{111}–rGO composite exhibited the best photo-catalytic performance. The kinetic results further confirmed the superiority of o-Cu_2O{1 1 1}–rGO. As shown in Fig. 3b, the degradation rate constants of o-Cu_2O–rGO, d-Cu_2O–rGO and c-Cu_2O–rGO catalysts were 0.651, 0.456 and 0.185 h^{-1}, respectively. Surprisingly, the degradation rate of o-Cu_2O–rGO was approximately three times higher than that of c-Cu_2O–rGO. The blank experiments were carried out (Fig. 3a) after stirring 2 h in dark, it was illustrated that the MB degradation could be neglected either under visible light without catalysts or with catalysts in dark, and thus the obtained photo-catalytic results were considered reasonable. The photo-catalytic activity of o-Cu_2O–rGO was higher than the two other composites, implying that the interaction of interconnected interface was crucial. Generally, the photo-catalytic activity of Cu_2O-based materials was greatly depended on surface area, light-adsorption, the recombination rate of photo-generated charge carriers, the stability of Cu^+ species and the oxygen defects [26,27]. Therefore, the interfacial effects on the properties of Cu_2O–rGO composites had been comprehensively investigated.

Nitrogen adsorption/desorption isotherms and pore size distributions of as-prepared Cu_2O–rGO composites were expressed in Fig. S3. All the composites had isotherms of type IV from the Brunauer–Deming–Deming–Teller (BDDT) classification [28], and the pore size distributions of Cu_2O–rGO were similar. From Table. S1, it was suggested that the difference in Cu_2O–rGO surface areas was negligible. Therefore, the surface area was not the key factor for the photo-catalytic performance. In addition, the surface area of o-, d-, c-Cu_2O crystals were 2.2, 2.4, 2.5 m^2/g, respectively. The introduce of graphene oxide (GO) increased the surface area of Cu_2O–reduced graphene oxide (rGO) composites, which indicated that the reduced graphene oxide was beneficial for the well-dispersion of Cu_2O crystals.

The optical absorption properties of graphene oxide (GO) and Cu_2O–rGO composites with different crystal facets were investigated by the comparison (Fig. S4a). Similar to Cu_2O samples (Fig. S4b), Cu_2O–rGO composites exhibited broad absorption in the visible-light region, while, graphene oxide displayed no noticeable absorption peaks for visible light, except for a peak at 300 nm corresponding to the π–π^* transition of oxygen-containing functional groups [29]. It was indicated that the introduction of Cu_2O was helpful for the visible-light adsorption. Furthermore, according to the three Cu_2O–rGO composites (magnification UV–vis DRS inserted in Fig. S4a), it could be found that the visible-light adsorption was ranked by o-Cu_2O–rGO > d-Cu_2O–rGO > c-Cu_2O–rGO, which illustrated that o-Cu_2O–rGO could make full use of sunlight. In the magnified spectra, the hump-like absorptions were caused by strong light scattering bands, and the scattering came from the relatively large size of Cu_2O nanocrystals [30,31]. The energy band of the Cu_2O–rGO composites were also analyzed by the plots of $(\alpha Ep)^2$ *vs* Ep (Ep = hc/λ, h: Planck constant, c: velocity of light, λ: absorption wavelength). The energy bands of o-Cu_2O–rGO, d-Cu_2O–rGO and c-Cu_2O–rGO were 1.80, 1.85 and 1.95 eV, respectively; and that of o-Cu_2O, d-Cu_2O and c-Cu_2O were 1.98, 2.02 and 2.04 eV, respectively. Thus, the rGO sheets made more influence on the energy band of o-Cu_2O–rGO composite, indicating that the interfacial structures between Cu_2O crystal facets and rGO sheets affected the energy band. The stronger interaction between o-Cu_2O {1 1 1} and rGO might exist, which enhanced

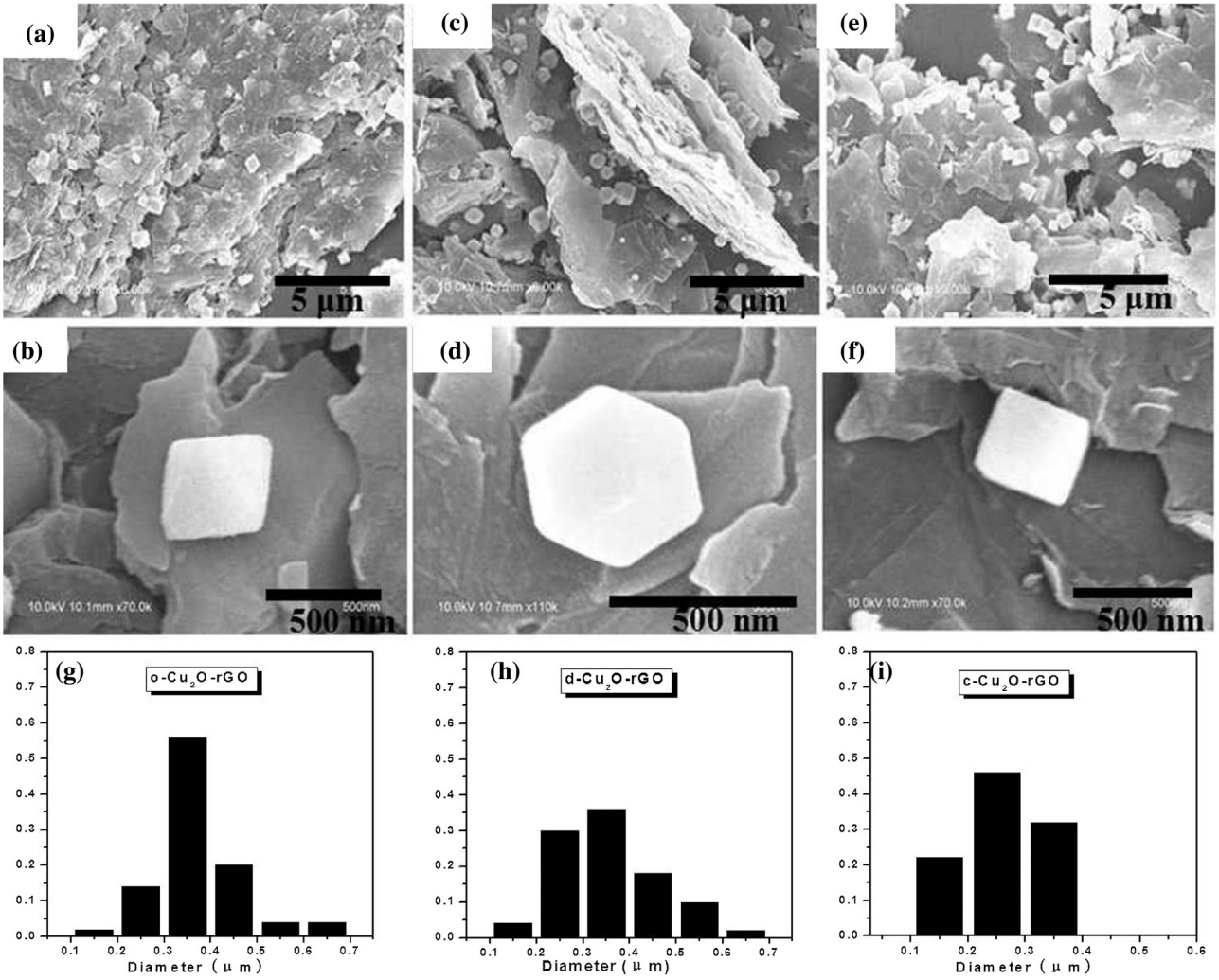

Fig. 2. SEM images of (a) (b) o-Cu_2O–rGO; (c) (d) d-Cu_2O–rGO; (e) (f) c-Cu_2O–rGO; the size distribution of (g) o-Cu_2O–rGO; (h) d-Cu_2O–rGO; (i) c-Cu_2O–rGO.

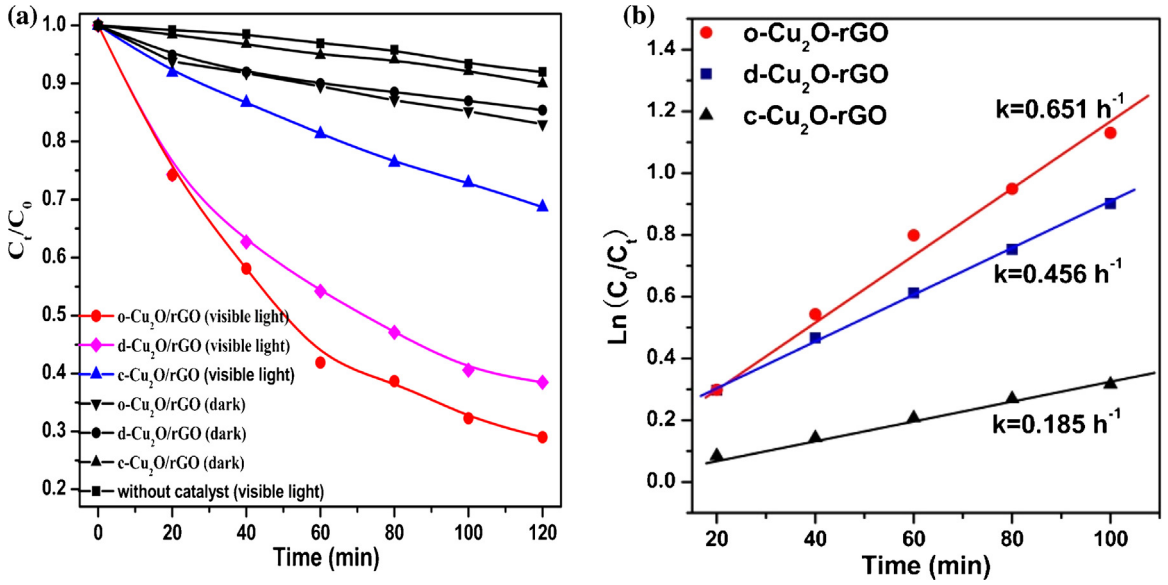

Fig. 3. (a) Degradation curves (including blank experiments) and (b) kinetic curves of methylene blue catalyzed by Cu_2O–rGO composites under visible light.

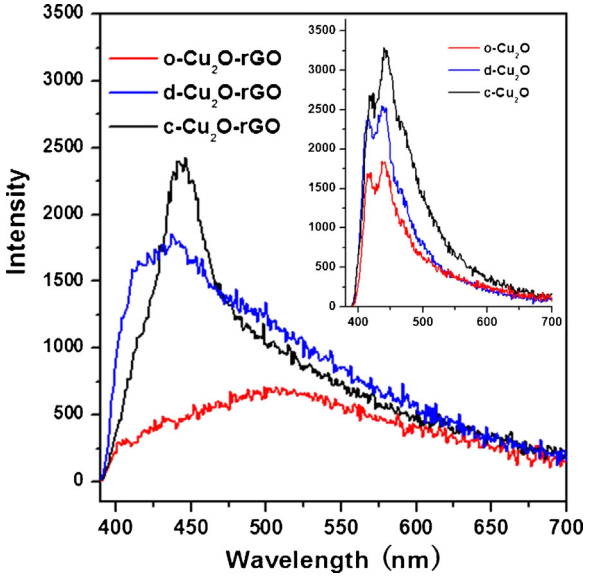

Fig. 4. PL spectra of Cu_2O–rGO composites; and PL spectra of Cu_2O with different shapes (insert graph).

visible light absorption of o-Cu_2O–rGO, and was facilitated to the photo-degradation.

Generally, photoluminescence (PL) spectra was a well known technique to investigate both transfer process of the interface charge carrier and the recombination process involved with the electron–hole pairs [32,33]. It was reported that the photoluminescence came from the following process. Light was absorbed by the material and the excess energy was given to the electrons, which caused the electrons within the material to move into permissible excited states. Afterwards, the electrons returned to their equilibrium states, and the light was emitted [34]. PL spectra were sensitive to energy level of the impurities, crystalline quality, and exciton structures, and thus the relative intensities of each peak in PL spectra could employ to determine the relative vacancy concentration and the corresponding recombination efficiency [31,35,36]. In this work, the interfacial charge-transfer process between different Cu_2O crystal facets and rGO sheets was investigated by PL spectra. As shown in Fig. 4, the broad peaks from 400 to 550 nm were corresponding to the electron transitions from the different sub-levels of conduction band to the Cu d-levels of the valence band [31,37]. Das et al. proposed that for the bare Cu_2O, the valence band (VB) were Cu 3 d, hybridized, Cu 3 d –4 s and O 2-p based on the theoretical calculations and experiment, and conduction band (CB) were Cu 4 s and 4p states. Furthermore, transitions from the top of VB to the bottom of CB (3 d–4 s) were forbidden according to selection rules, and the peak at 405 nm in Fig. 4 was ascribed to the top of VB to the top of conduction levels (3 d–4 p allowed transitions) [31]. In comparison of bare Cu_2O, the peak became broad for the Cu_2O-rGO composites, which might be resulted in the surface conjugation (d–π conjugate) of Cu_2O and rGO sheets, this similar phenomenon was also observed in TiO_2-graphene composite reported by Tu et al. [38]. According to the insert graph of Fig. 4, it was clearl that Cu_2O/rGO composites had the lower peak intensity than bare Cu_2O samples, implying that the introduction of rGO contributed to decreasing the recombination of electron–hole pairs. Furthermore, the PL intensities of three Cu_2O/rGO composites were ranked as: o-Cu_2O–rGO < d-Cu_2O–rGO < c-Cu_2O–rGO. The o-Cu_2O{1 1 1}–rGO composite displayed the lowest PL intensity, indicating that the recombination of photo-generated electrons and holes was the poorest, and the photo-generated electrons transferred rapidly to rGO sheets. It was deduced that the charge-transfer process of Cu_2O–rGO composites was dependent on the interfacial interaction between rGO sheets and Cu_2O crystal facets exposed. In addition, creating an interfacial contact between graphene and TiO_2 was reported, and the controlled interface was able to enhance the photo-catalytic performance [21,39]. Similarly, in this work, the stronger interaction between o-Cu_2O {1 1 1} facets and rGO could promote the properties of photo-catalysis.

Moreover, the interfacial electronic states of Cu_2O–rGO composites and rGO were measured by XPS. The chemical states of carbon were showed in Fig. 5a. The C 1s spectrum of pure GO and Cu_2O/rGO composites could be fitted into four peaks of *ca.* 284.6, 285.5, 286.6 and 288.4 eV, and these four peaks were assigned to elemental carbon, C—O of hydroxyl or epoxy groups, and O═C—O, respectively [21]. The oxygen containing groups (C—O and O═C—O) peaks of Cu_2O–rGO composites were similar to that of rGO, confirming that the graphene oxide had been substantially reduced in the preparation of Cu_2O–rGO composites, consistent with the XRD results. Amazingly, it could be found that the binding energy of C═C peak in o-Cu_2O–rGO was slightly lower than that of the two other Cu_2O–rGO composites (Table. S2). It was reported that the binding energy was related with the electronic structures [40]. Therefore, it was deduced that the electron-transfer interaction in o-Cu_2O–rGO sample was intensive, and this phenomenon was not observed in the two other Cu_2O–rGO composites.

On the other hand, the surface Cu species were also analyzed by XPS (in Fig. 5b). As mentioned in previous literatures, the primary peak at 934.4 eV and satellite peaks at 940.0 and 945.0 eV were ascribed to Cu^{2+}, and the peak with binding energy of 932.1 eV was assigned to Cu^+ species in Cu 2p XPS spectra [41]. Notably, the Cu^+ species amount of o-Cu_2O–rGO was much more than that of two other Cu_2O–rGO composites, whereas, the Cu^+ species amounts were almost identical in the bare Cu_2O samples with different shapes (Fig. S5). The content ratio of Cu^+/Cu^{2+} in Cu_2O–rGO composites was o-Cu_2O–rGO > d-Cu_2O–rGO > c-Cu_2O–rGO (Table. S2), indicating that o-Cu_2O–rGO composite was convenient to stabilize Cu^+ species, which was indispensable for photo-catalytic degradation [42]. However, in the above XRD results (Fig. 1), no diffraction peaks of CuO were detected, because XRD characterization was used to analyze the phase in the bulk, which was the overall information of the sample. While, the detection of XPS characterization was usually limited to a few atomic layers of the surface, and thus the information of the atoms in the bulk (>5 nm) was difficult to capture [43].

Furthermore, the information of defects in Cu_2O–rGO composites was described by Raman spectra (in Fig. 6). A weaker Raman peak at around 615 cm^{-1} could be observed, which was identified to the defects from the breakdown of the symmetry of Cu_2O crystal lattice [44]. According to the intensity of the peak, the concentration of defects followed the order: o-Cu_2O–rGO > d-Cu_2O–rGO > c-Cu_2O–rGO. Bai et al. investigated the role of oxygen defects in photo-activity over ZnO/graphene, and discovered that oxygen defect in ZnO was helpful to enhance the photo-catalytic performance [25]. Therefore, it was believed that different crystal facet structures and interfacial electronic properties had a contribution to the oxygen defects of Cu_2O–rGO composites, leading to the distinct photo-catalytic performances. Furthermore, the structure disorder of Cu_2O–rGO composites was investigated. In the case of graphene oxide, two main peaks of ~1350 and 1595 cm^{-1} were observed, which were the characteristic signals of disorder band associated with structural defects generated in graphene (D band) and the well ordered E_{2g} phonon scattering of sp^2 carbon atoms of graphene (G band), respectively [21]. Compared with graphene oxide, the positions of D band and G band in Cu_2O–rGO composites were slightly shifted, due to the reduction of graphene oxide and the combination of Cu_2O nanocrystals with rGO sheets. Previous studies had reported that the intensity ratio of I_D/I_G was proposed

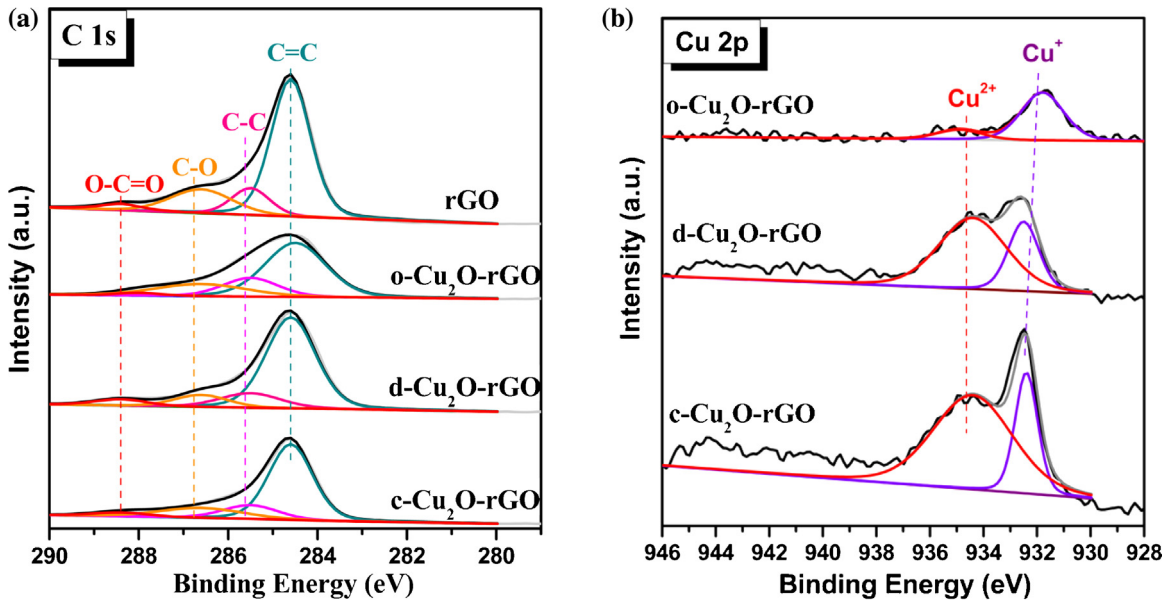

Fig. 5. XPS spectra of (a) C 1s region (b) Cu $2p_{3/2}$ region for Cu_2O–rGO composites.

to be an indication of structure disorder and defects in GO or rGO [21,45]. As showed in Fig. 6, the I_D/I_G ratios were from 0.90 to 1.31 in GO and Cu_2O–rGO composites, demonstrating the decrease in the average size of sp^2 domains and the reduction of GO to rGO [46]. On the basis of the discussion above, the stronger interaction between o-Cu_2O {1 1 1} and rGO was in favor of more generated oxygen defects, which promoted the photo-catalytic performance.

It was well known that the reactive oxide species played a decisive role in the pollutant degradation [25,47]. Thus, the *in-situ* ESR spin-trap technique was employed to determine the generated reactive oxide species during the irradiation with DMPO radical scavenger. Under visible light irradiation, the signals of the formed superoxide radical species for Cu_2O–rGO composites were displayed in Fig. 7. Only superoxide radicals ($O_2^{\bullet-}$) were appeared in methanol system with the characteristic six peaks [48], and the hydroxyl radicals (•OH) were not observed. The result showed

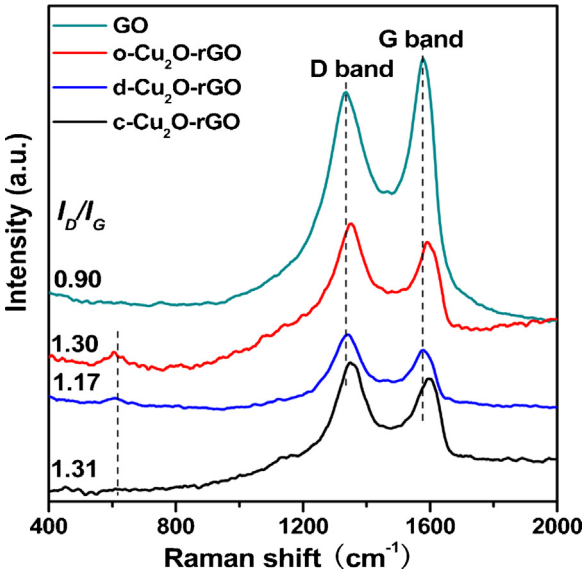

Fig. 6. Raman spectra of Cu_2O–rGO composites and graphene oxide.

that photo-degradation of MB dye was triggered by the electron mechanism, i.e., $O_2^{\bullet-}$ radicals generated through the activation of molecular oxygen in the process were the main active oxygen species in the photo-catalytic degradation. The signal peak of superoxide radical was first generated in o-Cu_2O–rGO after visible light irradiation for 2 min, whereas, for the two other composites, the signal peak were not found at the moment, which illustrated that o-Cu_2O–rGO exhibited more rapid enrichment of radicals. Thus, the larger amount and longer lifetime of superoxide radical ($O_2^{\bullet-}$) were conducive to the outstanding photo-catalytic activity of o-Cu_2O–rGO. The phenomenon further confirmed that the interfacial charge–transfer interactions between o-Cu_2O {1 1 1} and rGO were advantageous, photo-generated electrons rapidly transferred to rGO sheets, which were captured by adsorbed O_2 to form superoxide radicals, and then MB molecules were oxidized.

FT-IR spectra provided the structural information of Cu_2O–rGO composites and reduced graphene oxide (rGO). The characteristic vibration bands were shown in Fig. 8. It was reported that graphene oxide (GO) had abundant hydroxyl, carboxyl, epoxide groups, including C=O carboxylic acid vibration at 1750 cm^{-1}, O—H stretching vibration at 1420 cm^{-1}, C—OH stretching vibration at 1226 cm^{-1}, C—O stretching vibration of Ar—OH groups at 1080 cm^{-1} [8,49]. As for Cu_2O–rGO composites and rGO, the bands of oxygen containing groups were partially disappeared, indicating that the samples were efficiently reduced during the prepared process, in agreement with XRD and XPS results. The skeletal bending vibration of aromatic C=C at *ca.* 1600 cm^{-1} was remained, and the peaks of aromatic C=C were greatly different in Cu_2O–rGO composites and rGO. Compared with d-Cu_2O–rGO, c-Cu_2O–rGO and rGO, the peak position of o-Cu_2O–rGO was blue-shifted. Likewise, a band at *ca.* 650 cm^{-1} attributed to the Cu—O vibration was slightly red-shifted on o-Cu_2O–rGO composite. Previous studies showed that the peak position in FT-IR was closely related to the coordination environment and electronic structures of various functional groups [39,50]. Therefore, it was suggested that on the o-Cu_2O {1 1 1} and rGO interface, the interactions of interfacial charge transfer were the strongest, which was indicating that the π electrons of rGO sheet were facilitate to connect with Cu atom, weakening the Cu—O bond in o-Cu_2O (red-shifted Cu—O vibration of o-Cu_2O–rGO in FT-

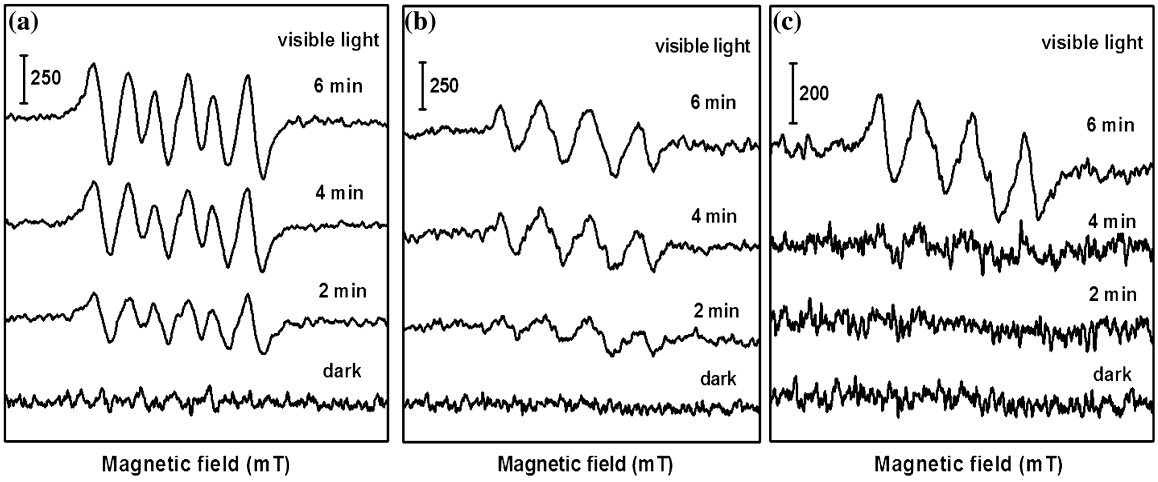

Fig. 7. ESR spectra of superoxide radical species over (a) o-Cu_2O–rGO, (b) d-Cu_2O–rGO (c) c-Cu_2O–rGO photo-catalysts under the irradiation of visible light ($\lambda > 420$ nm) (DMPO as the radical trapper).

IR) and then the stabilization of Cu^+; simultaneously, Cu atom had more d-electrons, donating to rGO sheet (blue-shifted C=C vibration of o-Cu_2O–rGO in FT-IR).

To further confirm that o-Cu_2O–rGO composite exhibited the superior photo-catalytic performance, the cycling tests of Cu_2O–rGO composites were carried out. The corresponding cycling results displayed in Fig. S6. It could be observed that after the four cycles, the degradation performance was not apparently declined over o-Cu_2O–rGO composite, in comparison with the two others. The results indicated that the stronger interfacial charge–transfer interactions between o-Cu_2O {1 1 1} and rGO was of great benefit to the degradation activity and stability of photo-catalysts. In addition, the cycling degradation tests of different-shaped Cu_2O were showed in Fig. S7. Their activities were poor, for the reason of the photo-corrosion of Cu^+ in the process [51]. The above discussions verified that Cu_2O–rGO composites were better than Cu_2O catalysts, and o-Cu_2O–rGO composite was outstanding. Furthermore, the used Cu_2O–rGO composites after four recycling experiments were determined by XPS and XRD characterization. The valence states of the surface copper species were displayed in Fig. S8a. The content ratio of Cu^+/Cu^{2+} in Cu_2O–rGO composites was calculated in Table. S3, ranked by o-Cu_2O–rGO > d-Cu_2O–rGO > c-Cu_2O–rGO. It was observed that the surface Cu^{2+} species of the used Cu_2O–rGO composites after four recycling experiments was increased. However, from the XRD results (Fig. S8b), all the diffraction patterns of Cu_2O crystals were ascribed perfectly to the pure cubic-phase Cu_2O, and no other copper species (Cu or CuO) were detected. According to the fact that XRD result was the information of the sample in whole, it was deduced that rGO sheet was able to stabilize the Cu_2O crystals after four recycling experiments.

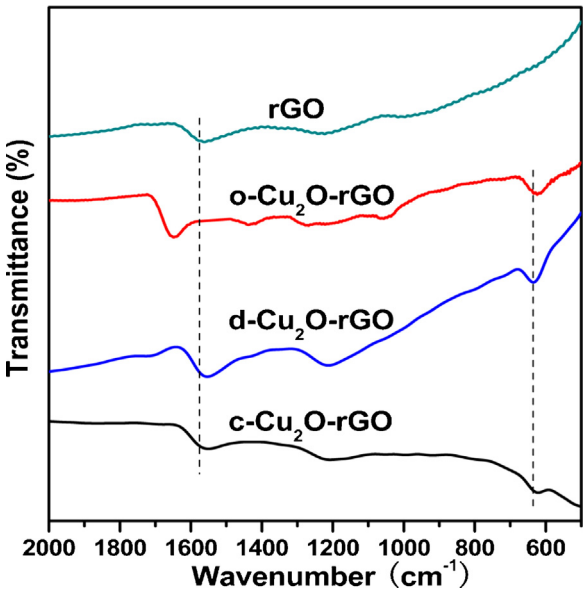

Fig. 8. FT-IR spectra of Cu_2O–rGO composites and reduced graphene oxide.

Based on the above experimental results, it was considered that superoxide radical played a direct effect on the oxidation of MB. In the initial stage of the MB degradation, the visible light was adsorbed by the Cu_2O–rGO composite, leading to the generation of electrons (e^-) and holes (h^+); afterwards, the electrons were transferred to rGO sheets on interface, captured by adsorptive O_2 on rGO sheets. The formed electrophilic $O_2^{\bullet-}$ attacked the positive-charged MB molecules, resulted in the oxidation of MB molecules to hydrocarbon compounds through ring opening reaction, and finally oxidized into CO_2 and H_2O. On the basis of the process, the superoxide radicals ($O_2^{\bullet-}$) exerted an important role in the photo-activity. Furthermore, the generation of $O_2^{\bullet-}$ were affected by many factors, i.e., the light-absorption, the rapid transferred rate of photo-generated electrons, the Cu^+ species and oxygen defect, which were influenced by the interfacial connections between Cu_2O crystal facets and rGO sheets.

Therefore, the possible schematic illustration of the interfaces between rGO and different Cu_2O crystal facets was proposed. In Fig. 9, it was clear that coordinated unsaturated O (O_{CUS}) entirely existed on interfaces between Cu_2O {1 1 1} {1 1 0} {1 0 0} and rGO sheets. Considering of the photo-activity results, O_{CUS} on the interfaces were not the key factor. Notably, the Cu coordination environments on the interfaces were different. For o-Cu_2O{1 1 1}–rGO, the coordinated unsaturated Cu (Cu_{CUS}) were present on interface. While, for d-Cu_2O{1 1 0}–rGO and c-Cu_2O{1 0 0}–rGO, there were only coordinated saturated Cu (Cu_{CSA}). Generally, Cu_{CUS} was more active than Cu_{CSA}, leading to the stronger interfacial contact with rGO sheets, and then o-Cu_2O–rGO had the best photo-catalytic performances. In comparison with the interfaces of d-Cu_2O–rGO and c-Cu_2O–rGO composites, the Cu_{CSA} was present on the first layer of d-Cu_2O {1 1 0} facet, but was not on the first layer of c-Cu_2O {1 0 0} facet, this kind of steric effect resulted in the different photo-catalytic performances. Therefore, o-Cu_2O–rGO composite displayed the superior photo-catalytic activity, d-Cu_2O–rGO composite was followed, and c-Cu_2O–rGO composite was the poorest.

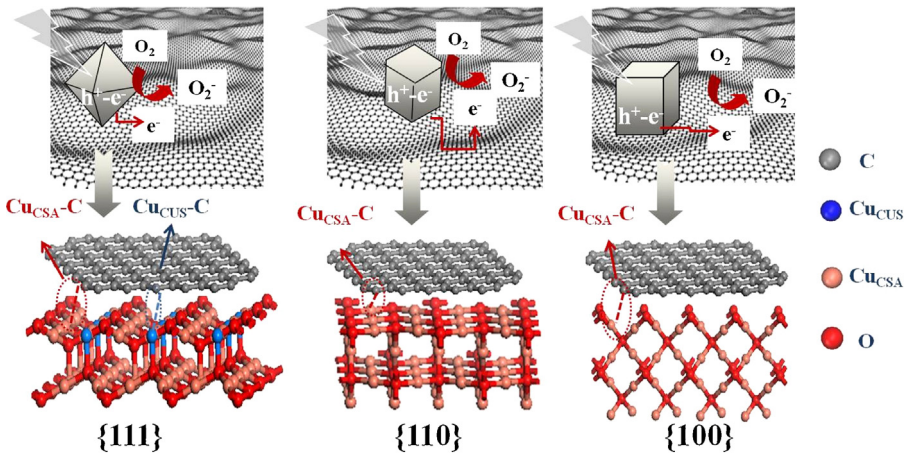

Fig. 9. Schematic illustration of atomic structures of interfaces between rGO and different Cu_2O crystal facets and the photo-degradation of methylene blue.

4. Conclusion

Cu_2O–rGO composites were synthesized with tunable Cu_2O crystal facets ({1 1 1}, {1 1 0} and {1 0 0} facets). The prepared composites had similar particle sizes and surface areas. In the photo-catalytic degradation of methylene blue under visible light, o-Cu_2O{1 1 1}–rGO showed the superior performance, d-Cu_2O{1 1 0}–rGO was followed, and c-Cu_2O{1 0 0}–rGO was the poorest. UV–vis diffuse reflectance and photoluminescence spectra showed that o-Cu_2O{1 1 1}–rGO exhibited the enhanced visible-light absorption and the faster charge-transfer rate. Furthermore, FT-IR, X-ray photoelectron spectroscopy and Raman characterizations confirmed that due to advantageous electronic structures and interfacial connections of o-Cu_2O{1 1 1}–rGO, the Cu^+ species and oxygen defects were much easier to exist. *In-situ* ESR study showed that the larger amount and longer lifetime of superoxide radicals ($O_2^{\bullet-}$) were present over o-Cu_2O–rGO composite. The above results confirmed that the superior photo-activity of o-Cu_2O–rGO composite came from the advantageous interface between o-Cu_2O {1 1 1} and rGO sheets. For the highly-active coordinated unsaturated Cu on the interface, the interfacial interactions were intensified and photo-generated electrons rapidly transferred to rGO sheets, and the electons were captured by adsorbed O_2 to generate the superoxide radicals ($O_2^{\bullet-}$), which oxidized the MB molecules. These results indicated that engineering the interfacial structures of the Cu_2O–rGO composites could provide a strategy to design excellent photo-catalysts. This method could be extended to other materials related to graphene for high efficient photo-catalytic materials.

Acknowledgements

Financial supports from the Natural Science Foundation of Jiangsu Province (BK2012298) and National Natural Science Foundation of China (Nos. 21273110, 21203091) were gratefully acknowledged.

Appendix A. Supplementary data

Supplementary data associated with this article can be found, in the online version, at http://dx.doi.org/10.1016/j.apcatb.2015.08.017.

References

[1] M.R. Hoffmann, S.T. Martin, W.Y. Choi, D.W. Bahnemannt, Chem. Rev. 95 (1995) 69–96.
[2] F. Dong, A. Suda, T. Tanabe, Y. Nagai, H. Sobukawa, H. Shinjoh, M. Sugiura, C. Descorme, D. Duprez, Catal. Today 90 (2004) 223–229.
[3] C.C. Chen, W.H. Ma, J.C. Zhao, Chem. Soc. Rev. 39 (2010) 4206–4219.
[4] W.C. Huang, L.M. Lyu, Y.C. Yang, M.H. Huang, J. Am. Chem. Soc. 134 (2012) 1261–1267.
[5] A.D. Handoko, J.W. Tang, Int. J. Hydrogen Energy 38 (2013) 13017–13022.
[6] A. Paracchino, V. Laporte, K. Sivula, Nat. Mater. 10 (2011) 456–461.
[7] S. Sahoo, S. Husale, B. Colwill, T.M. Lu, S. Nayak, P.M. Ajayan, ACS Nano 3 (2009) 3935–3944.
[8] S. Deng, V. Tjoa, H.M. Fan, J. Wei, C.H. Sow, J. Am. Chem. Soc. 134 (2012) 4905–4917.
[9] L.C. Liu, X.R. Gu, C.Z. Sun, H. Li, Y. Deng, F. Gao, L. Dong, Nanoscale 4 (2012) 6351–6359.
[10] W.C. Wang, L.M. Lyu, M.H. Huang, Chem. Mater. 23 (2011) 2677–2684.
[11] L.L. Wang, J. Ge, A.L. Wang, J. Jiang, Q. Zhang, Y. Luo, Y.J. Xiong, Angew. Chem. Int. Ed. 53 (2014) 5107–5111.
[12] B.J. Li, H.Q. Cao, G. Yin, Y.X. Lu, J.F. Yin, J. Mater. Chem. 21 (2011) 10645–10649.
[13] J. Chen, S.H. Shen, P.H. Guo, M. Wang, L.J. Guo, Appl. Catal. B: Environ. 152 (2014) 335–341.
[14] Q. Xiang, J. Yu, M. Jaroniec, Chem. Soc. Rev. 41 (2012) 782–796.
[15] H.L. Wang, L.S. Zhang, Z.G. Chen, J.Q. Hu, J.S. Liu, X.C. Wang, Chem. Soc. Rev. 43 (2014) 5234–5244.
[16] C. Lee, X. Wei, J.W. Kysar, J. Hone, Science 321 (2008) 385–388.
[17] H.C. Gao, Y.X. Wang, F. Xiao, C.B. Ching, H.W. Duan, J. Phys. Chem. C 116 (2012) 7719–7725.
[18] X.Q. An, K.F. Li, J.W. Tang, ChemSusChem 7 (2014) 1086–1093.
[19] T. Wu, M.X. Chen, L. Zhang, X.Y. Xu, Y. Liu, J. Yan, W. Wang, J.P. Gao, J. Mater. Chem. A 1 (2013) 7612–7622.
[20] P.D. Tran, S.K. Batabyal, S.S. Pramana, J. Barber, L.H. Wong, S.C.J. Loo, Nanoscale 4 (2012) 3875–3878.
[21] L.C. Liu, Z. Liu, A.N. Liu, X.R. Gu, C.Y. Ge, F. Gao, L. Dong, ChemSusChem 6 (2013) 1–11.
[22] L.Z. Zhang, J.W. Shi, M.C. Liu, D.W. Jing, L.J. Guo, Chem. Commun. 50 (2014) 192–194.
[23] P. Rai, R. Khan, S. Raj, S.M. Majhi, K.K. Park, Y.T. Yu, I.H. Lee, P.K. Sekhar, Nanoscale 6 (2014) 581–588.
[24] Z.J. Fan, K. Wang, T. Wei, J. Yan, L.P. Song, B. Shao, Carbon 48 (2010) 1686–1689.
[25] X.J. Bai, L. Wang, R.L. Zong, Y.H. Lv, Y.Q. Sun, Y.F. Zhu, Langmuir 29 (2013) 3097–3105.
[26] L.W. Zhang, H.B. Fu, Y.F. Zhu, Adv. Funct. Mater. 18 (2008) 2180–2188.
[27] W. Wang, J. Yu, Q. Xiang, B. Cheng, Appl. Catal. B: Environ. 119 (2012) 109–117.
[28] C. Sun, L. Liu, L. Qi, H. Li, H. Zhang, C. Li, F. Gao, L. Dong, J. Colloid Interface Sci. 364 (2011) 288–297.
[29] K. Krishnamoorthy, R. Mohan, S.J. Kim, Appl. Phys. Lett. 98 (2011) 144103–244101.
[30] C.H. Kuo, M.H. Huang, J. Phys. Chem. C 112 (2008) 18355–18360.
[31] K. Das, S.K. De, J. Lumin. 129 (2009) 1015–1022.
[32] X. Xing, R. Liu, X. Yu, G. Zhang, H. Cao, J. Yao, B. Ren, Z. Jiang, H. Zhao, J. Mater. Chem. A 1 (2013) 1488–1496.
[33] K.K. Haldar, G. Sinha, J. Lahtinen, A. Patra, ACS Appl. Mater. Interfaces 4 (2012) 6266–6274.
[34] A.M. White, E.W. Williams, P. Porteous, C. Hilsum, J. Phys. D: Appl. Phys. 4 (1970) 1322–1328.
[35] H. Shi, K. Yu, Y. Wang, Q.J. Wang, Z.Q. Zhu, Appl. Phys. A 108 (2012) 709–717.
[36] W.L. Yu, K. Jiang, J.D. Wu, J. Gan, M. Zhu, Z.G. Hu, J.H. Chu, Phys. Chem. Chem. Phys. 13 (2011) 6211–6218.

[37] J.P. Dahl, A.C. Switendick, J. Phys. Chem. Solids 27 (1966) 931–938.
[38] W.G. Tu, Y. Zhou, Q. Liu, Z.P. Tian, J. Gao, X.Y. Chen, H.T. Zhang, J.G. Liu, Z.G. Zou, Adv. Funct. Mater. 22 (2012) 1215–1221.
[39] J.S. Lee, K.H. You, C.B. Park, Adv. Mater. 24 (2012) 1084–1088.
[40] C.Y. Ge, L.J. Liu, X.J. Yao, C.J. Tang, F. Gao, L. Dong, Catal. Sci. Technol. 3 (2013) 1547–1557.
[41] A.L. Cámara, M. Monte, A. Martínez-Arias, J.C. Conesa, Catal. Sci. Technol. 2 (2012) 2436–2439.
[42] Z.K. Zheng, B.B. Huang, Z.Y. Wang, Y. Dai, J. Phys. Chem. C 113 (2009) 14448–14453.
[43] M.J. Genet, C.C. Dupont-Gillain, P.G. Rouxhet, Med. Appl. Colloids (2008) 177–307.
[44] M. Ivanda, D. Waasmaier, A. Endriss, J. Ihringer, A. Kirfel, W. Kiefer, J. Raman Spectrosc. 28 (1997) 487–493.
[45] S. Stankovich, D.A. Dikin, R.D. Piner, K.A. Kohlhaas, A. Kleinhammes, Y. Jia, Y. Wu, S.T. Nguyen, R.S. Ruoff, Carbon 45 (2007) 1558–1565.
[46] G.K. Pradhan, D.K. Padhi, K. Parida, ACS Appl. Mater. Interfaces 5 (2013) 9101–9108.
[47] J.Y. Jing, Y. Zhang, W.Y. Li, W.W. Yu, J. Catal. 316 (2014) 174–181.
[48] D.T. Sawyer, J.S. Valentine, Acc. Chem. Res. 14 (1981) 393–400.
[49] T.B. Tessy, S. Ramaprabhu, J. Phys. Chem. C 115 (2011) 8527–8533.
[50] T. Venkov, K. Hadjiivanov, Catal. Commun. 4 (2003) 209–213.
[51] L. Huang, F. Peng, H. Yu, H. Wang, J. Solid State Sci. 11 (2009) 129–135.